View metadata, citation and similar papers at core.ac.uk

brought to you by CORE

provided by CiteSeerX

July 30-August 2, 2007 San Diego, California USA

FEDSM2007-37351

NUMERICAL INVESTAGATION OF GAS-SOLID SUSPENSION FLOW IN 180° CURVED DUCT

K. A. Ibrahim
Faculty of Engineering, Minoufiya University,
Shebin El-kom, Egypt.

M. A. El-Kadi
Faculty of Engineering, Minoufiya University,
Shebin El-kom, Egypt.

Mofreh H. Hamed
Faculty of Engineering, Kafr Elsheikh University,
Kafr Elsheikh, Egypt.
mofrehhh@yahoo.com

Samy M. El-Behery
Faculty of Engineering, Minoufiya University,
Shebin El-kom, Egypt.
s_elbehery@yahoo.com

ABSTRACT

In this paper, a two-way coupling Eulerian-Lagrangian approach is presented for the simulation of gas-solid two-phase flow in 180° curved duct. In the present study, Reynolds averaged Navier-Stokes equations (RANS) and two turbulence models namely; standard k-ε model and RNG (Renormalization Group) based k-ε model are adopted. The effects of particle rotation and lift forces are included in the particle tracking model while the effect of inter-particle collisions is neglected. The present predictions are compared with published experimental data for single-phase flow and published particles trajectories. The comparisons show that the RNG based k-ε model predicts the flow behaviour better than the standard k-ε model. Furthermore, the particles trajectories are compared very well with published data. The effects of inlet gas velocity, bend geometry, loading ratio and solid properties on the flow behaviour are also discussed. The results show that the flow behaviour is greatly affected by the above parameters.

Keywords: Gas-solid, U-bend, Pneumatic conveying, Numerical simulation

INTRODUCTION

Bends are a common element in any piping system of gas-solid flow applications such as pneumatic conveyers, pneumatic dryers, chemical industries and food processing. The gas-solid flow in bends is affected by complex parameters, such as centrifugal forces, formation and dispersion of ropes, secondary flows and erosion of bend outer walls. The gas-solid flow in 90° bend has been studied by many researchers. Levy and Mason [1] and Huber and Sommerfeld [2] studied the effect of the bend on the cross-sectional particle concentration and segregation of solid particles from the carrier gas. Ibrahim et al. [3] studied the characteristics of gas-solid flow in a horizontal-to-horizontal 90° bend and they continued their work [4] to investigate the effect of bend orientation and flow direction on the behavior of gas-solid flow through bends. The roping phenomena was investigated experimentally in vertical-to-horizontal 90° bend by McCluskey et al [5] and Jakobsen et al. [6], while Yilmaz and Levy [7] studied this phenomena in horizontal-to-vertical 90° bend. The effect of 90° bends on the system pressure drop was investigated by Ratnayaka et al. [8] and McGlinechey et al. [9] for dense phase pneumatic conveying and by Chaudhry et al. [10] for lean phase pneumatic conveying. The U-bend is a basic element of pneumatic dryers and heat exchangers. Hidayat and Rasmuson [11-13] investigated numerically the gas-solid flow in circular U-bend using Eulerian model for both phases. The mass loading ratio used in the investigation was varied from 0.001 to 0.01. Niu and Tsao [14] evaluated the erosion due solid impact in a two-dimensional curved channel. From the previous discussion it is clear that the behavior of gas solid flow in U-bend needs to be investigated to evaluate the effect of flow parameters on the characteristics of such flows. Therefore, the aim of this paper is to investigate numerically the flow of gas-solid suspension in U-bend in order to evaluate the ability of existing computational methods to simulate such flows.

NOMENCLATURE

D	Diameter of bend, m
D_p	Particle diameter, μm
e	Restitution coefficient
Mr	Mass loading ratio, $(\dot{m}_p / \dot{m}_g)$
P	Pressure, N/m^2
R_C	Mean bend radius of curvature, m
t	Time, sec
u, v	Mean axial and radial velocities, m/s
$\bar{U}, \bar{U}_p$	Normalized mean axial gas and particle velocities
u_{p1}, v_{p1}	Mean axial and radial particle velocities before impact, m/s
u_{p2}, v_{p2}	Mean axial and radial particle velocities after rebound, m/s
U_o	Mean-bulk longitudinal velocity, m/sec

Copyright © 2007 by ASME

$\bar{y}$	Normalized distance measured from the inner
x	Axial coordinates along the straight ducts

Greek symbols

α	Gas phase void fraction
β	Solid phase void fraction
δ	Curvature ratio ($D/2R_c$)
θ	Axial coordinate along the bend, degree
Φ	General dependent variable
μ	Viscosity, $N.s/m^2$
ρ	Density, kg/m^3
ω_p	Particle angular velocity, rad/s

Subscripts

1	before impact
2	after rebound
p	Particle

GOVERNING EQUATIONS

The numerical calculations of particle-laden gas flow in 180° bend are performed using Eulerian approach for gas-phase, taking into account the mutual effects of the solids on the air, and Lagrangian approach for dispersed-phase. In the present study all the particles have been introduced in the flow with approximately the same bulk velocity of the fluid. The particulate phase consists of spherical particles.

Fluid Flow Modelling

The gas flow calculations are based on the Reynolds averaged Navier-Stokes (RANS) equations in connection with two turbulent models namely standard k-ε model and RNG based k-ε model. Following Refs. [15-16], the elliptic differential equations governing two-dimensional, turbulent, steady, incompressible and isothermal flow through 180° bend shown in Fig. 1 are as follow:

Continuity equation

$$\frac{\partial}{\partial x_i}(\alpha\rho u_i)=0.0 \tag{1}$$

Momentum equation

$$\frac{\partial}{\partial x_j}(\alpha\rho u_i u_j)=-\frac{\partial}{\partial x_i}(\alpha P)+\frac{\partial}{\partial x_j}\left\{\alpha\mu_{eff}\left(\frac{\partial u_i}{\partial x_j}+\frac{\partial u_j}{\partial x_i}\right)\right\}+S_P^{u_i} \tag{2}$$

Turbulent kinetic energy

$$\frac{\partial}{\partial x_j}(\alpha\rho u_j k)=\frac{\partial}{\partial x_j}\left\{\alpha\frac{\mu_{eff}}{\sigma_k}\frac{\partial k}{\partial x_j}\right\}+\alpha(G-\rho\varepsilon)+S_P^k \tag{3}$$

where

$$G=\mu_{eff}\left(\frac{\partial u_i}{\partial x_j}+\frac{\partial u_j}{\partial x_i}\right)\frac{\partial u_i}{\partial x_j} \tag{4}$$

Dissipation rate

$$\frac{\partial}{\partial x_j}\left(\alpha\rho u_j\varepsilon\right)=\frac{\partial}{\partial x_j}\left\{\alpha\frac{\mu_{eff}}{\sigma_\varepsilon}\frac{\partial\varepsilon}{\partial x_j}\right\}+\frac{\alpha\varepsilon}{k}\left(C_1G-C_2\rho\varepsilon\right)-\alpha\rho R+S_P^\varepsilon \tag{5}$$

In the above equations, the parameter Φ represents the variables u_i, k and ε, while, S_P^Φ is the source terms due to the presence of dispersed phase. The constants of the two turbulence models are given in table 1. The effective and eddy viscosities are calculated for standard k- ε (model-1) and RNG based k- ε (model-2) as in reported Refs. [15 and 16], respectively as,

Standard k-ε, model

$$\mu_{eff}=\mu+\mu_t \quad , \quad \mu_t=C_\mu\rho\frac{k^2}{\varepsilon} \tag{6}$$

RNG based k-ε model

$$\mu_{eff}=\mu\left[1+\sqrt{\frac{C_\mu\rho}{\mu}}\frac{k}{\sqrt{\varepsilon}}\right]^2 \quad , \quad \mu_t=\mu_{eff}-\mu \tag{7}$$

The Prandtl number, σ_k and σ_ε in the RNG bases k-ε model are calculated as follows,

$$\left|\frac{\lambda-1.3929}{\lambda_o-1.3929}\right|^{0.6321}\left|\frac{\lambda+2.3929}{\lambda_0+2.3929}\right|^{0.3679}=\frac{\mu}{\mu_{eff}} \tag{8}$$

where, λ is an inverse Prandtl number with λ_o=1.

The rate of strain R in the ε equation of RNG based k- ε model is expressed as given in [16] by,

$$R=\frac{C_\mu\eta^3\left(1-\eta/\eta_o\right)\varepsilon^2}{(1+\chi\eta^3)k} \tag{9}$$

and

$$\eta=\frac{k}{\varepsilon}\left(2S_{ij}^2\right)^{\frac{1}{2}} \quad ,S_{ij}=\frac{1}{2}\left(\frac{\partial u_i}{\partial x_j}+\frac{\partial u_j}{\partial x_i}\right) \tag{10}$$

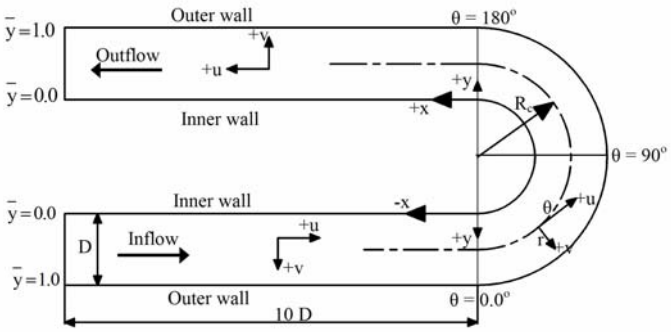

Fig. 1 Schematic view of 180° curved duct and coordinate system.

Particle Phase Modelling

The solid phase is treated by the Lagrangian approach, a few thousands of computational particles 'parcels' were traced through the flowfield in each coupling iteration. After each given time step the new position of the parcels and the new translation and angular velocities are calculated from the equations of motion as in [15] through,

$$\frac{d\vec{X}_p}{dt}=\vec{U}_p \tag{11}$$

$$m_p\frac{d\vec{U}_p}{dt}=\vec{F}_D+\vec{F}_{SL}+\vec{F}_{LM} \tag{12}$$

$$I_p\frac{d\vec{\omega}_p}{dt}=\vec{T} \tag{13}$$

$$\vec{T}=\pi\mu D_p^3\left[\frac{1}{2}\nabla\times\vec{U}-\vec{\omega}_p\right] \tag{14}$$

Copyright © 2007 by ASME

where, $\vec{X}_P$ is the particle position vector, $\vec{U}$, $\vec{U}_P$ are the gas and particle velocity vectors, $\vec{\omega}_P$ is the particle angular velocity vector, T is the torque acting on the particle, Ip is moment of inertia and, m_p is the particle mass, $\vec{F}_D$, $\vec{F}_{SL}$ and $\vec{F}_{LM}$ are the components of the force arising from drag, shear lift and Magnus lift due to particle rotation, respectively, and calculated as follows,
The drag force is calculated from:

$$F_D = \frac{3}{4}\frac{\rho\ m_p}{\rho_p D_p} C_D \left(\vec{U}-\vec{U}_p\right)\left|\vec{U}-\vec{U}_p\right| \quad (15)$$

where C_D is the drag coefficient and calculated as given by [17].

The slip shear lift force is based on the analytical result of Saffman [18] and extended for higher Reynolds numbers according to Mei [19]:

$$\vec{F}_{SL} = 1.615.D_p\mu\,Re_s^{0.5}\,C_{SL}\left[(\vec{U}-\vec{U}_p)\times\vec{\omega}_f\right] \quad (16)$$

where, $\vec{\omega}_f = 0.5(\nabla\times\vec{U})$ is the fluid rotation, while, $Re_S = \rho D_p^2|\omega_f|/\mu$ is the particle Reynolds number of the shear flow and the $C_{SL} = F_{sl}/F_{sl,Saff}$ represents the ratio of the extended lift force to the Saffman force:

$$\begin{aligned} C_{SL} &= (1-0.3314\gamma^{0.5})e^{-Re_p/10} + 0.3314\gamma^{0.5} \qquad Re_p \le 40 \\ &= 0.0524(\gamma\,Re_p)^{0.5} \qquad Re_p > 40 \end{aligned} \quad (17)$$

where γ is the correction function proposed by [19] and is defined as,

$$\gamma = \frac{Re_s}{0.5\,Re_p} \quad (18)$$

The Magnus lift due to particle rotation is expressed as in [15] by,

$$\vec{F}_{LM} = \frac{1}{2}\rho\vec{V}_r^2\frac{\pi D_p^2}{4}C_{LM}\frac{\vec{\omega}_r\times\vec{V}_r}{\left|\vec{\omega}_r\right|\left|\vec{V}_r\right|} \quad (19)$$

Where the quantities $\vec{V}_r = \vec{U}-\vec{U}_p$ and $\vec{\omega}_r = \vec{\omega}_f - \vec{\omega}_p$ are the local relative linear and angular velocities between fluid and the particle, respectively. The Magnus lift coefficient may be expressed as in [15] by,

$$\begin{aligned} C_{LM} &= \frac{D_p\left|\vec{\omega}_r\right|}{\left|\vec{V}_r\right|} \qquad Re_p \le 1 \\ &= \frac{D_p\left|\vec{\omega}_r\right|}{\left|\vec{V}_r\right|}\left(0.178+0.822\,Re_p^{-0..522}\right) \quad 1 < Re_p < 1000 \end{aligned} \quad (20)$$

Table (1) Constants values of the two used models.

Model	C_μ	σ_k	σ_ε	χ	η_o	C_1	C_2
Standard k-ε model	0.09	1.0	1.3	-	-	1.44	1.92
RNG based k-ε model	0.0845	Eqn.(8)	Eqn.(8)	0.015	4.38	1.42	1.68

Effect of Particles on Gas Flow

The particles occupy the computational cell and reduce the gas volume fraction and exert interaction forces on the surrounding gas phase. Thus, the two phases are coupled through the gas volume fraction and through the total source term, S_p^ϕ that accounts for the momentum transfer from the particles to the gas (two-way coupling).
The void fraction for dispersed phase, β and for gas phase, α are calculated using trajectory method, Ref. [20] as,

$$\beta = \sum_{traj}\frac{n_k\Delta t_k V_p}{V_c} \quad , \quad \alpha = 1-\beta \quad (21)$$

where, n_k is the number of actual particles in the computational parcel (k), V_P is the volume of the particle, V_c is the volume of computational cell and $\sum_{traj}$ means summing over all trajectories passing through the computational cell. The source term of dispersed phase in the gas momentum equation is calculated as in [15] by,

$$S_p^{u_i} = \frac{\beta\rho_p}{m_p\,n}\sum_{k=1}^{n}\left(\vec{F}_{D_k}+\vec{F}_{LR_k}+\vec{F}_{SL_k}\right) \quad (22)$$

where, n is the number of trajectories passing through the computational cell. The effect of particulate phase on the turbulent structure can be neglected in standard k-ε model for equilibrium gas-solid flow of high density ratio [15. While in RNG based k-ε model the particulate phase affect the turbulent structure and it can be written as reported in [16] for k and ε equations, respectively, as follow,

$$S_p^k = 2.k\left[\frac{\rho_p}{\tau_p}\right]\left[1-\exp(-B_k\frac{\tau_p}{\tau_l}\right] \quad (23)$$

$$S_p^\varepsilon = 2.\varepsilon\left[\frac{\rho_p}{\tau_p}\right]\left[1-\exp(-B_\varepsilon\frac{\tau_p}{\tau_l}\right] \quad (24)$$

where B_k, B_ε are constants and taken as 0.09 and 0.4 respectively as in [16]. While, $\tau_l = k/\varepsilon$ and τ_P is the particle relaxation time.

Inlet and Boundary Conditions

At the inlet, the axial velocity profile for gas phase is assumed fully developed turbulent velocity profile, where the radial velocity is assumed to be zero. At outlet, the gradient of flow variables in the flow direction; $\partial\Phi/\partial x = 0$ (Neumann conditions), and the radial velocity v is set to zero. At the solid wall boundaries, however, $u = v = 0.0$, no-slip conditions.

$$k_{in} = 0.003\,U_0^2 \quad , \quad \varepsilon_{in} = C_\mu\frac{k_{in}^{3/2}}{0.01.D} \quad (25)$$

Because the k and ε equations are not solved at the grid point adjacent to the wall, a modelling scheme is required to simulate the variation of eddy viscosity, μ_t. For this purpose the mixing length approach is adopted where the eddy viscosity is modelled as a function of mixing length as in Ref. [21].

$$\mu_t = \rho\,\ell_m^2\left[\left(\frac{\partial u_i}{\partial x_j}+\frac{\partial u_j}{\partial x_i}\right)\frac{\partial u_i}{\partial x_j}\right]^{1/2} \quad (26)$$

where ℓ_m is the mixing length. For smooth walls it is calculated from Van Driest`s equation, [21] as,

$$\ell_m = Ky_p\left(1-\exp(-y^+/A)\right) \quad (27)$$

Where, A is a constant equal to 26 for smooth walls in the equilibrium near wall layer. Also to improve the accuracy of RNG based k- ε the second-order finite difference formula is used to evaluate the velocity gradient at the wall. This can be written as, in [22] as,

$$\left(\frac{\partial u}{\partial y}\right)_w = \frac{-8u_w+9u_1-u_2}{3y_w}+O(y_w^2) \quad (28)$$

where, y_w is the thickness of the cell adjacent to the wall. While $u_w = 0.0$ for stationary wall and no slip condition, u_1

Copyright © 2007 by ASME

and u_2 are the velocities at the next two grid points, respectively.

Particle Wall Interaction

The condition of rebound is achieved if the particle velocity before collision, w_{p1} is greater than the critical particle velocity, $w_{p,cr}$ as in Ref. [23]. The solution of the momentum equations with Coulombs law of friction yields a set of equations for sliding and non-sliding collision process [24]. The condition for non-sliding collision is,,

$$\left| u_{p1} - \frac{D_p}{2}\omega_{p1} \right| \le \frac{7}{2}\mu_o(1+e)v_{p1} \qquad (29)$$

Here, the subscript 1 refers to the particle velocities before impact, μ_o is the static coefficient of friction. The values of restitution and friction coefficients are taken as 0.9 and 0.4, respectively as in Ref. [24] for all calculations.

SOLUTION PROCEDURE AND CONVERGENCE

Finite volume discretization and iterative solution, based on the SIMPLE algorithm by Ref. [25], have been used for the numerical solution of the fluid phase. The calculations are performed with a mesh of control volumes shown in Fig. 2. The iterative procedure is repeated until convergence is achieved, (the normalized residuals for all variables, summed over the whole calculation domain, were each smaller than 0.001). In order to handle the interaction between the gas and the particles, calculations of the particle trajectories by integrating the translational and rotational equation of motion for each parcel in a small time step Δt using fourth order Runge-Kutta method are performed. With the computed information on the particles, the solid phase source term and void fractions can be calculated and introduced into the gas equations using suitable under-relaxation factor before the solution procedure is repeated. The overall procedure is repeated until the maximum error in the axial gas velocity between two successive coupled iterations is less than 0.005 of the inlet mean velocity.

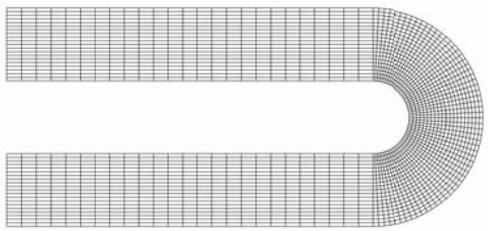

Fig. 2 Computational domain for 180^o curved duct.

MODEL VALIDATIONS

The U-bend of Monson and Seegmiller [26] is a strongly curved internal flow problem. The geometry consists of a straight constant area duct leading to a 180 degree bend with constant gap spacing followed by another straight constant area duct. Reynolds number was 10^5 based on the inlet mean gas velocity and duct height. The experiment was conducted for CFD validation purposes. The predicted axial gas velocity profiles are compared with experimental data of [26] as shown in Fig. 3. The figure shows that the RNG based k-ε model predict the axial velocity better than the standard k-ε model near the outer wall in the upstream duct and up to the bend inlet , the latter predicted better than the former near the inner wall in the tested range. Inside the bend and up to $\theta = 30^o$ both model predicted the axial velocity very well, as the flow progresses both models under predict the axial velocity near the outer wall up to $\theta = 150^o$. At the exit from the bend, separation region begins to appear and continued to x/D =1. Therefore, it is evident to conclude that, RNG k-ε model accurately predicts this region than standard k-ε model. Downstream the separation region the RNG k-ε model still predict the axial velocity better than the standard k-ε model up to x/D = 12. At this section the flow has recovered from curvature effect and both models have nearly the same behavior. In general, the predictions by RNG k-ε model were found to be in acceptable agreement more than that of the standard k-ε model. Therefore, the RNG k-ε model is used in the present two-phase flow simulations. The numerical results of [14] are selected for 180^o bend validations. The predicted trajectories for 50, 100 and 200 μm particle sizes were compared with that of [14] and a good agreement is obtained as shown in Fig. 4

RESULTS

The turbulent gas-solid two-phase flow through 180^o bend is investigated numerically using RNG based k-ε model. The effects of curvature ratio δ, inlet gas velocity U_o, particle diameter D_p, mass loading ratio Mr and particle density, (ρ_p) on the flow behaviour studied. To analyze the calculation results, the axial gas velocity for the two phases are presented at several positions along the upstream duct, 180^o bend and the downstream duct for the parameter given in table 2, as shown in Figs. 5- 9.

Table 2 Summary of parameters used in bend calculations.

D_p, μm	ρ_p, kg/m^3	Mr, kg/kg	U_o, m/sec	δ
60	1680	0.2	15*	0.135
100*	2650*	0. 5*	20	0.33*
150	3950	1.0	25	0.5

* Base case.

Effect of Curvature Ratio

The curvature ratio is one of the key parameter for obtaining successful design of pneumatic bend. The curvature ratio plays a vital role in creating and controlling the particle rope. The effect of curvature ratio on the development of axial velocity profiles is shown in Fig. 5. The figure shows that the axial velocity for the gas phase increases near the inner wall and its maximum value being more and more as the curvature ratio increases. This is may be due to the increase in the radial pressure gradient with the increase in curvature ratio. Downstream the bend midsection ($\theta = 90^o$), axial velocity for gas phase begins to decrease near the inner wall due to the unbalance between the radial pressure gradient and centrifugal forces, consequently a separation region appeared near the inner wall downstream the bend exit for the sharp bend . On the other hand, the curvature ratio has a great effect on the particles flow. Thus, the slip velocity between the two phases increases, and the rope dispersion process occurs at a faster rate as the curvature ratio increases. This is due to the increase in impact and rebound angles as the curvature ratio increases. Furthermore, the accumulation of particles near the inner outer wall increases as the curvature ratio decreases which in turn results in a decrease in the axial gas velocity.

Copyright © 2007 by ASME

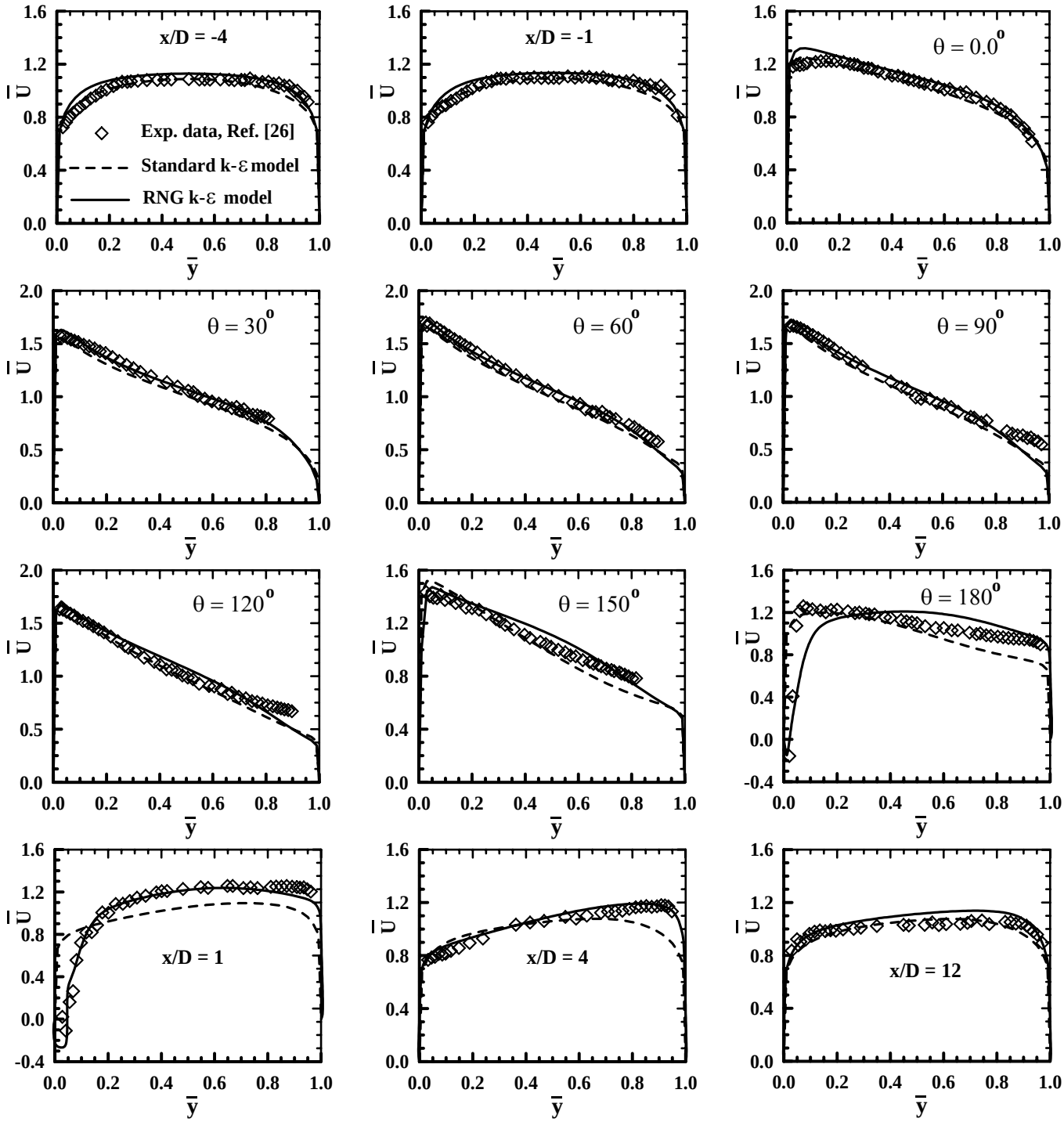

Fig. 3 comparisons between predicted normalized axial velocity profiles and published data of Monson and Seegmiller [26].

Effect of Inlet Gas Velocity

The effect of inlet gas velocity on the flow behaviour is also studied by changing the inlet gas velocity with respect to the base case as shown in Fig. 6. The figure indicates that the axial velocity profiles for the gas phase is less affected by the inlet gas velocity. On the other hand, the slip velocity between the two phases increases as the inlet gas velocity increases. Furthermore, the rope dispersion process occurs at a faster rate as the inlet gas velocity increases. This may be due to the increase in particles inertia and impact angle with the increase in inlet gas velocity.

Effect of Mass Loading Ratio

Figure 7 shows the effect of mass loading ratio on the axial gas velocity profiles for both phases. It can be seen from the figure that the axial velocity for the gas phase is increased near the outer wall as mass loading ratio increases, up to $\theta = 90^{o}$. This may be due to the increases in momentum transfer from solid phase to gas phase because the velocity of solids is grater than that of gas phase in this region. Downstream the bend midsection, the negative slip region is disappeared and the momentum begins to transfer from gas phase to the solid phase, consequently the axial velocity begins to decrease near the outer wall. As a result of the momentum exchange, the gas phase has recovered from mass loading effect approximately at bend exit (i.e.

Copyright © 2007 by ASME

the energy that transferred to the gas phase from the solid phase in the first half of the bend has been lost in the second half). As a result of the continuous energy lost from the gas phase, the axial velocity for both phases decreases near the outer wall and its decease being more and more as the mass loading ratio increases.

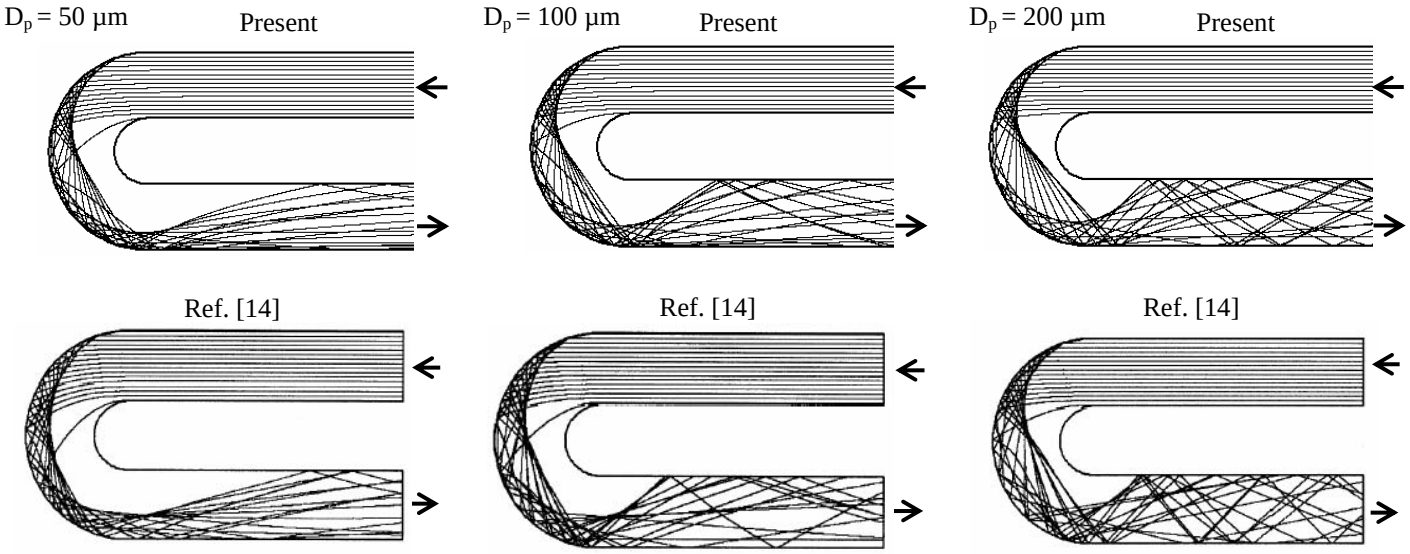

Fig. 4 Comparisons between predicted particle trajectories and published ones of Ref. [14].

Effect of Particle Diameter

The axial velocity profiles for both phases are presented in Fig. 8 for three different particles diameters. The figure indicates that, the slip velocity between the two phases increases as the particle diameter increases. Thus, the axial velocity of solids reaches about 0.5 U_o for the 150 µm particles size while it is about 0.8 U_o for the 60 µm particles size, as shown in the figure, at $\theta = 60^o$. This is may be due to the increase in particles segregation towards the outer wall as the particles size increases. Furthermore, the axial velocity for the 60 µm particles size does not changed suddenly after particle-wall collision, this may be due to that, the small particles responding to the change in the local flow velocity field and the change in its direction due to wall collisions is relatively small. Due to the effect of particle-wall interaction the solid velocity for all sizes reaches about 0.8 U_o at the bend exit. As the flow progresses in the downstream duct, the solid particles re-entrained into the bulk flow and the propagation of large particles occurs at a rate greater than that of smaller particles. Therefore, flat velocity profile for the large particles is obtained, which in turn results in more uniformity in the associated gas velocity profiles.

Effect of Particle Density

The effect of particle density on the axial velocity profiles for both phases is shown Fig. 9. The figure indicates that, as the particle density increases the slip velocity between the two phases increases. Thus, the slip velocity is about 0.5 U_o for the heaviest particles (ρ_p = 3970 kg/m^3) while it was about 0.2 U_o for the lightest ones (ρ_p = 1680 kg/m^3). As the flow progresses, due to particle-wall collision, the solids axial velocity reaches abut 0.8 U_o at the bend exit. In the downstream duct, the effect of centrifugal force on the particles motion is disappeared, and the rate of energy transfer from gas phase to solid phase increases, consequently the gas phase axial velocity at the outer wall slightly decreases. The figure indicates also that, the decrease in the axial velocity for gas velocity increases as the particle density decreases. This is due to that, the lighter particles accumulates at the outer wall more than the heavier ones.

CONCLUSIONS

Two particulate turbulence models have been used to predict the behaviour of turbulent gas-solid flows in U-bends taking into account the mutual effects. The effect of inlet gas velocity, particle diameter and density, curvature ratio and mass loading ratio on the flow parameters were demonstrated. The comparisons with single-phase flow data show that, the second model (RNG) illustrated a good agreement. Furthermore, the predicted particles trajectories by the present model show a very good agreement when it compared with the previous published ones. The present results help to understand the physical phenomena occurring in gas-solid flows in 180^o bends. It is senn that, the slip velocity and rope formation and dispersion processes are greatly affected by the gas flow and solid parameters.

REFERENCES

[1] Levy A. and Mason D. J., "The effect of a bend on the particle cross-section concentration and segregation in pneumatic conveying systems", Powder Tech., Vol. 98, 1998, pp. 95-103.

[2] Huber N., Sommerfeld M., "Characterization of the cross-sectional particle concentration distribution in pneumatic conveying systems. Powder Tech., Vol. 79, 1994, pp. 191-210.

[3] Ibrahim K. A.., El-kadi M. A., Hamed M. H. and El-Behery S. M., "Numerical simulation gas-solid two-phase flow in curved duct", Proceedings of ASME ATI'

Copyright © 2007 by ASME

Conference, "Energy: Production, Distribution and Conservation", Milan, Italy, May 14-17, 2006.Vol. 2, pp 981-990.

[4] Ibrahim K. A., El-kadi M. A., Hamed M. H. and El-Behery S. M., "Effect of bend orientation and flow direction on the behaviour of gas-solid flow ", Proc. 8th Int. Conf. of Fluid Dynamics and Propulsion, December 14-17, 2006, Sharm El-Shiekh, Sinai , Egypt, paper No. ICFD8-EG-136.

[5] McCluskey D. R., Easson W. J., Grated C. A. and Glass D. H., "The use of particle image velocimetry to study roping in pneumatic conveyance", Particle and Particle Systems Characterization, Vol. 6, 1989, pp. 129-132.

[6] Jakobsen M. L., McCluskey D. R., Easson W. J., Glass D. H. and Grated C. A., "Pneumatic particle conveyance in pipe bend: simultaneous two-phase PIV measurements of the slip velocity between the air and particle-phases", Proc. 7th Int. Symp. on Applications of Laser Techniques to Fluid Mechanics, Lisbon, Portugal, July 11-14, 1994.

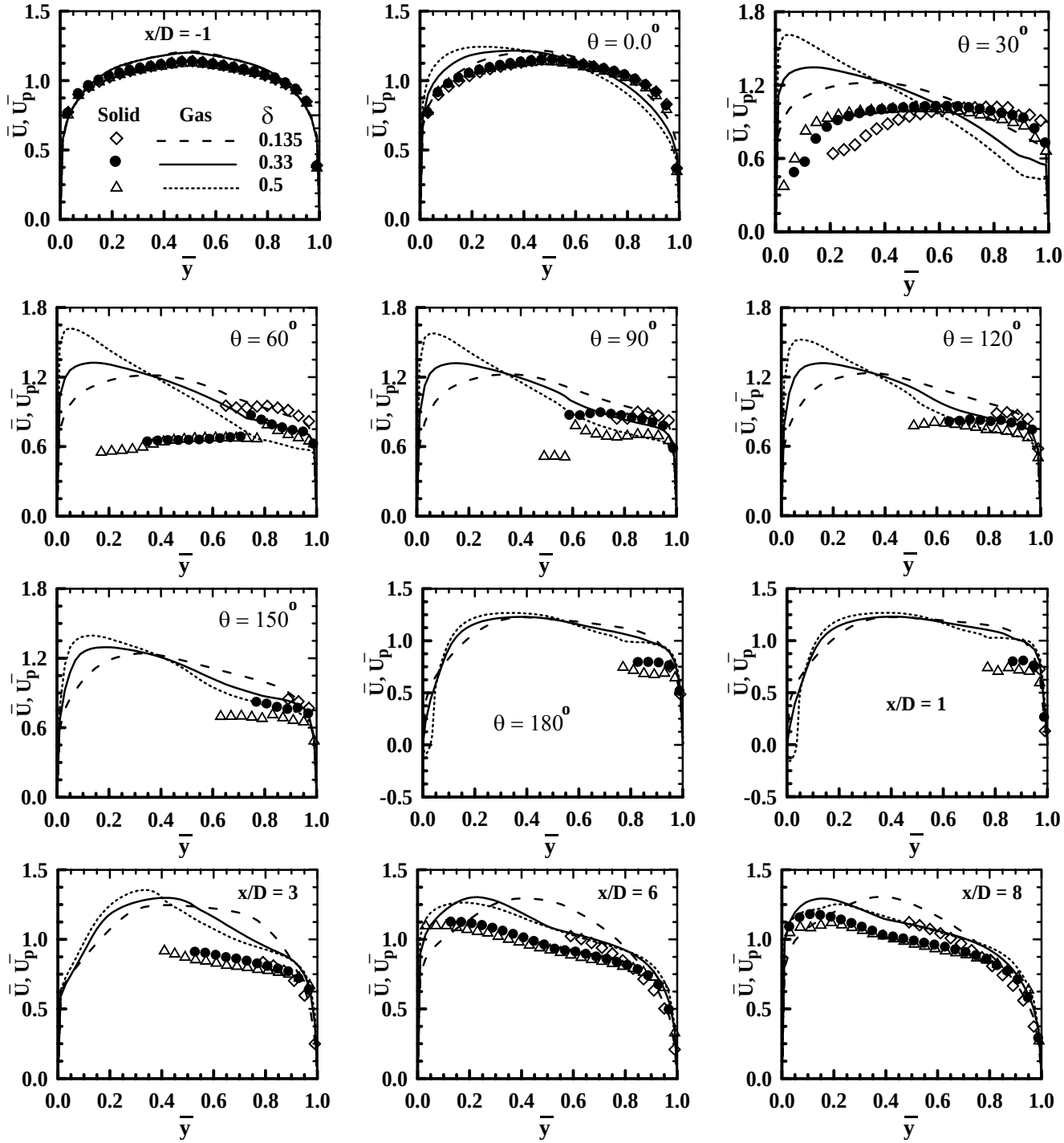

Fig. 5 Effect of curvature ratio, δ on the normalized axial velocity for both phases.

[7] Yilmaz A. and Levy E. K., "Roping phenomena in pulverized coal conveying lines", Powder Tech., Vol. 95, 1998, pp. 43-48.

[8] Ranayaka C., Melaaen M. c. and Datta B. K., "An experimental investigation and CFD modeling of gas-solid flow across a bend in a dense phase pneumatic conveying

Copyright © 2007 by ASME

system", Proc. 8th Int. Conf. on Bulk Material Storage, Handling and Transportation, Wollongong, Australia, 2004.
[9] McGlinchey D., Cowell A., Knight E. A., Pugh J. R., Mason A. and Foster B., "Bend pressure drop predictions using the Euler model in dense phase pneumatic conveying", Proc. Particulate System Analysis 2005, Stratford-upon-Avon, UK, Sept. 21-23, 2005.
[10] Chaudhry A. R., Bradley M. S. A., Hyder L. M., Reed A. R., and Farinsh R. J., "Analysis and modeling of bend pressure losses in lean phase pneumatic conveyors, for a range of particulate material", Proc. 7th Int. Conf. on Bulk Material Storage, Handling and Transportation", Newcastle, Australia, Oct. 2001.
[11] Hidayat M. and Rasmuson A., "Numerical investigation of gas-solid flow in a U-bend", Proc. of the 13th Int. Drying Symp., IDS' 2002, Beijing, China, August 27-30, 2002, Vol. A, pp. 424-433.
[12] Hidayat M. and Rasmuson A., "Numerical assessment of gas-solid flow in a U-bend", IchemE Trans., Part A, Chemical Engineering Research and Design, Vol. 82(A3), 2004, pp 332-343.
[13] Hidayat M. and Rasmuson A., "Some aspects on gas-solid flow in U-bend: Numerical investigation", Powder Tech., Vol. 153, 2005, pp. 1-12.
[14] Niu Y.-Y. and Tsao J.-C., "Numerical evaluation of erosion in curved duct", Numerical Heat Transfer, Part A, Vol. 41, 2002, pp. 341-356.
[15] Lun C. K .K. and Liu H. S., "Numerical simulation of dilute turbulent gas-solid flows in horizontal channels", Int. J. Multiphase flow, Vol. 23, 1997, pp. 575-605.
[16] Eghlimi A., Kouzoubov A., Fletcher C. A. J., " A new RNG-based two-equation model for predicting turbulent gas-particle flows", Proc. 1st Int. Conf. on CFD in Mineral & Metal Processing and Power Generation Industries, Melbourne, Australia, July 3-4, 1997.
[17] Kladas, D. D. and Deorgiou, D. P., " A Relative Examination of CD – Re Relationships used in Particle Trajectory Calculations ", Trans. of ASME, J. of Fluids Engineering, Vol. 115, pp. 162-165, 1993.
[18] Saffman P. G., "The lift on a small sphere in a slow shear flow", J. Fluid Mech., Vol. 22, Part 2, 1965, pp. 385-400.
[19] Mei R., "An approximate expression for the shear lift force on a spherical particle at finite Reynolds number", Int. J. Multiphase Flow, Vol. 18, 1992, pp. 145-147.
[20] Crowe C., Sommerfeld M. and Tsuji Y., "Multiphase flow with droplets and particles", CRC Press, Florida, USA, 1998.
[21] FLUENT theory manual, "Turbulence modelling, Section 10-7 [online]", Available at http://www.shef.ac.uk/mecheng/staff/xyl/fidap/help/theory/th10_03-08.htm#th1007 [accessed Jan., 21, 2006].
[22] Anderson J.D., Jr., "Computational fluid dynamics ", McGraw Hill Inc., 1995.
[23] Heinl E. and Bohent M., "Calculation of particle-wall adhesion in horizontal gas-solid flow using CFD", Powder Tech., Vol. 159, 2005, pp. 95-104.
[24] Sommerfeld M. and Huber N., "Experimental analysis and modelling of particle-wall collisions", Int. J. Multiphase Flow, vol. 25, 1999, pp. 1457-1489.
[25] Patankar S. V., "Numerical heat transfer and fluid flow", McGraw-Hill, New York, USA, 1983.
[26] Monson D. J. and Seegmiller H. E., "An experimental investigation of subsonic flow in a two-dimensional curved duct", NASA Technical Memorandum 103931, 1992.

Copyright © 2007 by ASME

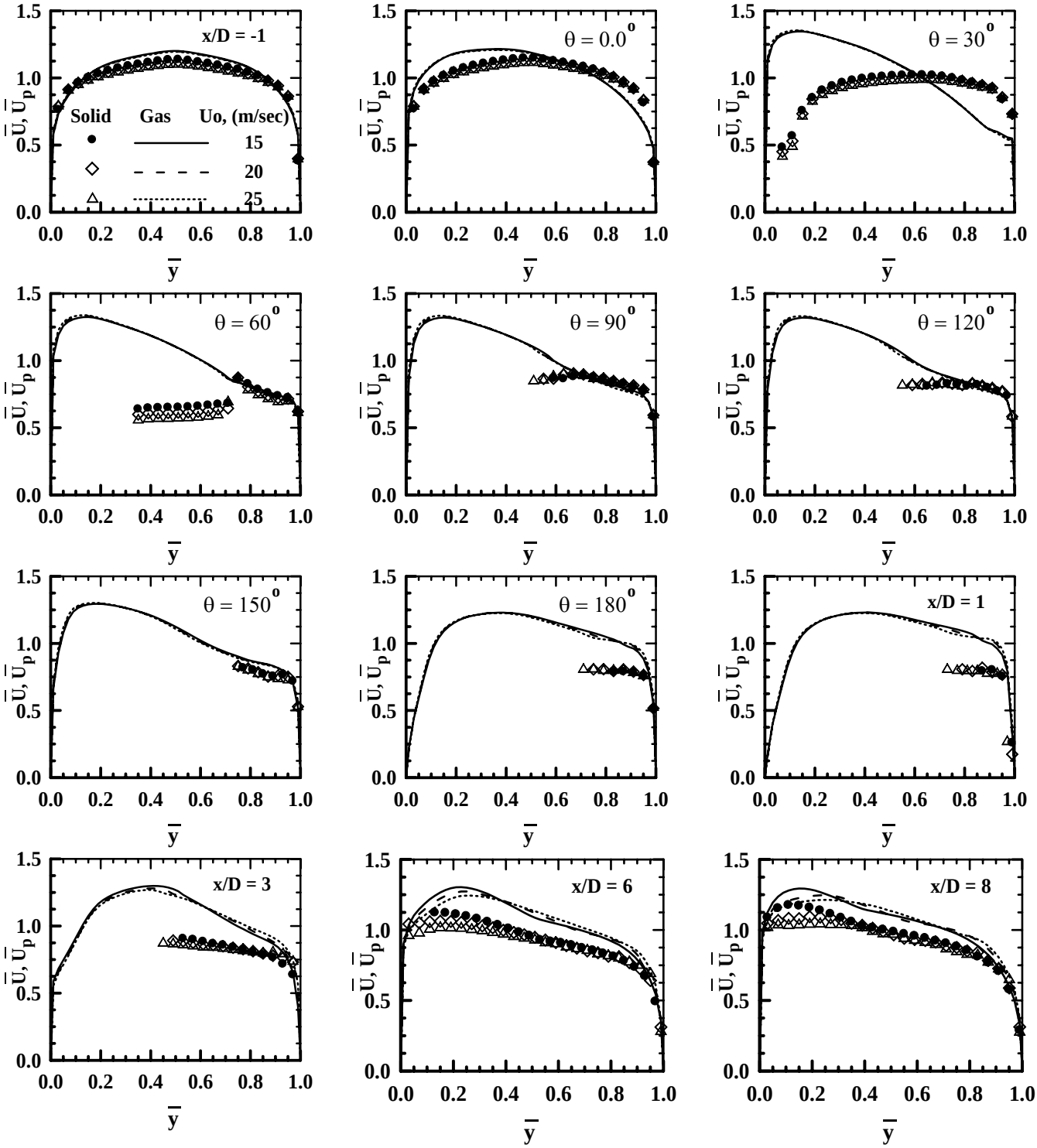

Fig. 6 Effect of inlet gas velocity, U_o on the normalized axial velocity profiles for both phases.

Copyright © 2007 by ASME

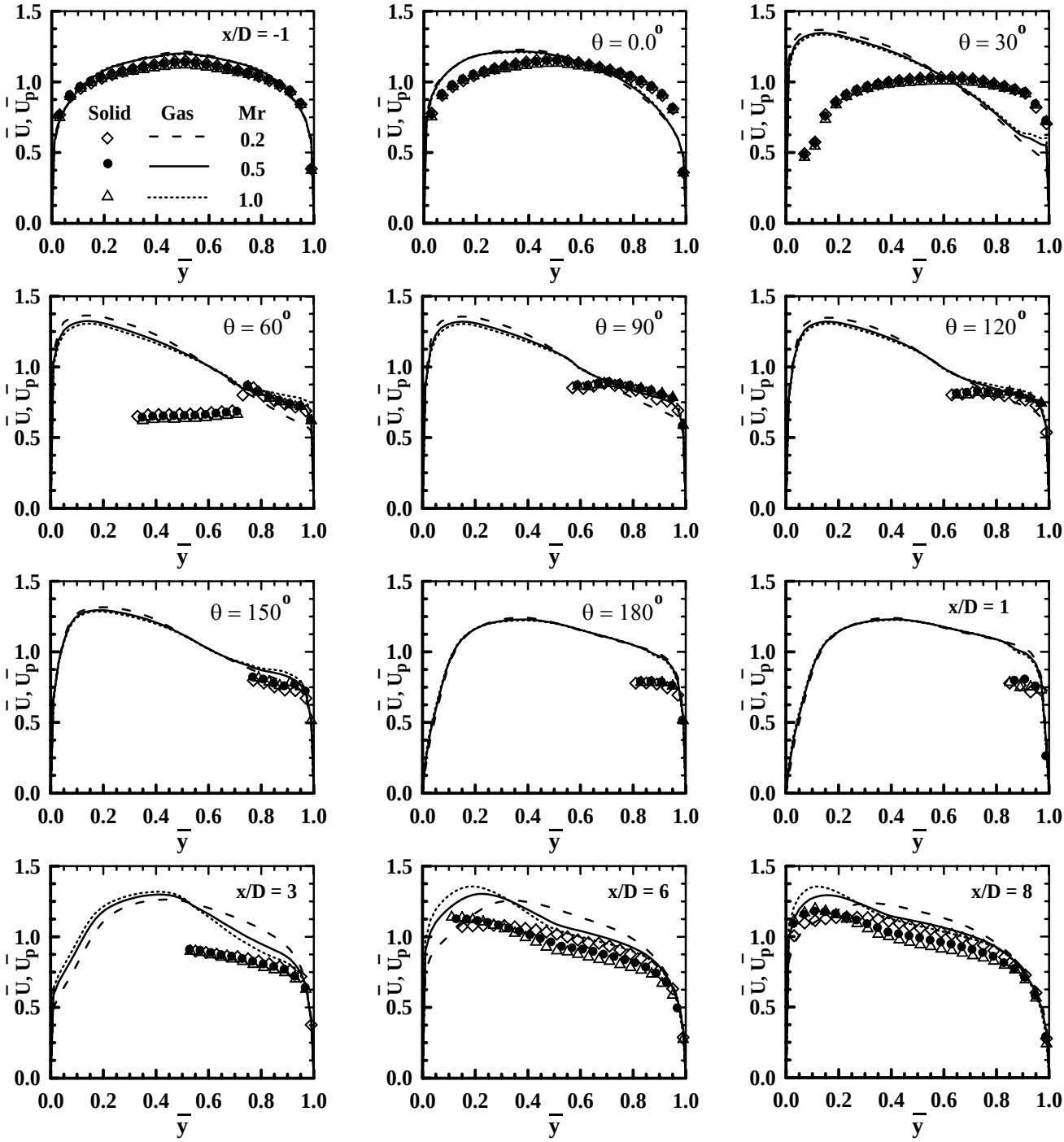

Fig. 7 Effect of mass loading ratio, Mr on the normalized axial velocity profiles for both phases.

Copyright © 2007 by ASME

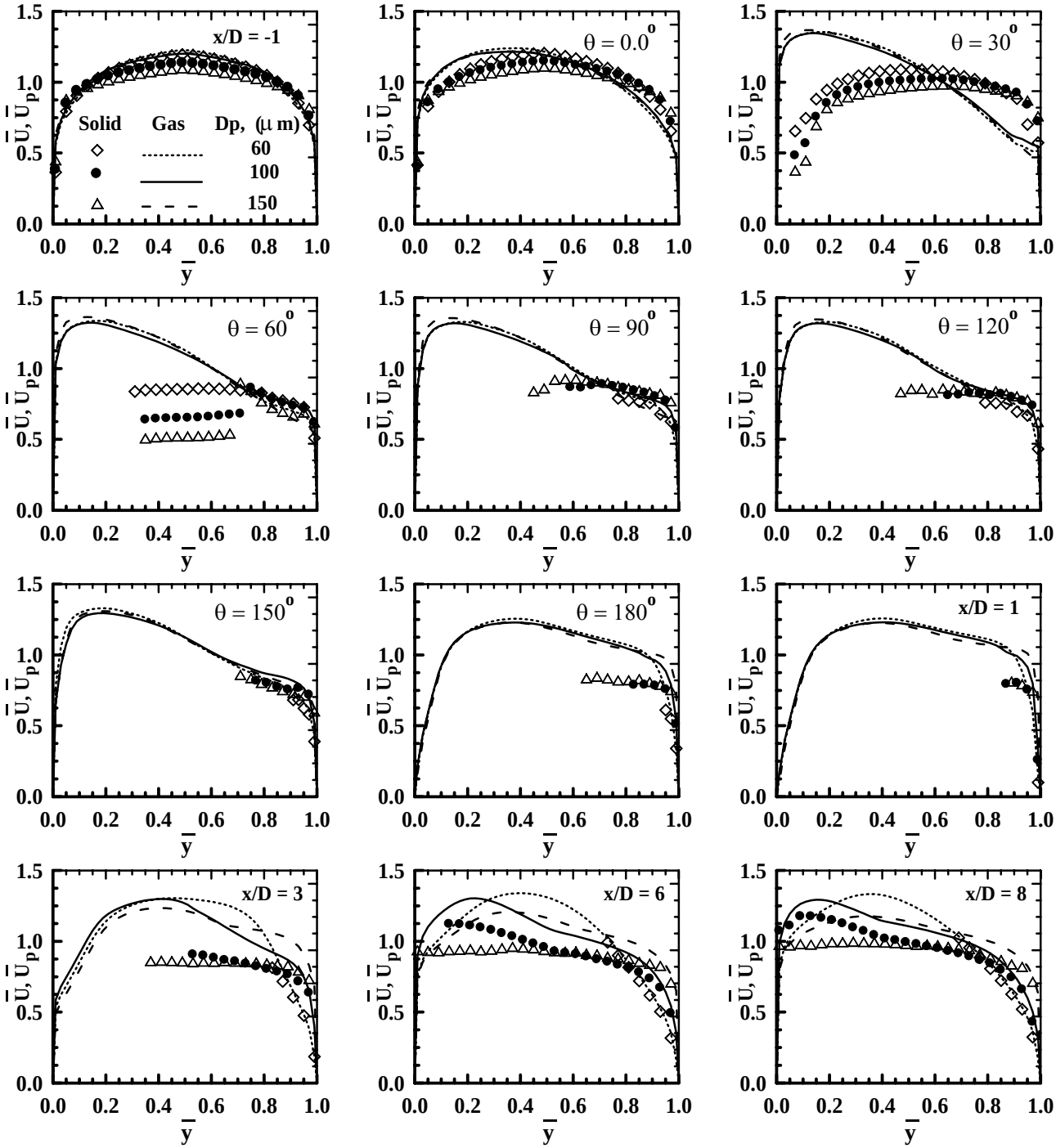

Fig. 8 Effect of particle diameter, D_p on the normalized axial velocity profiles for both phases.

Copyright © 2007 by ASME

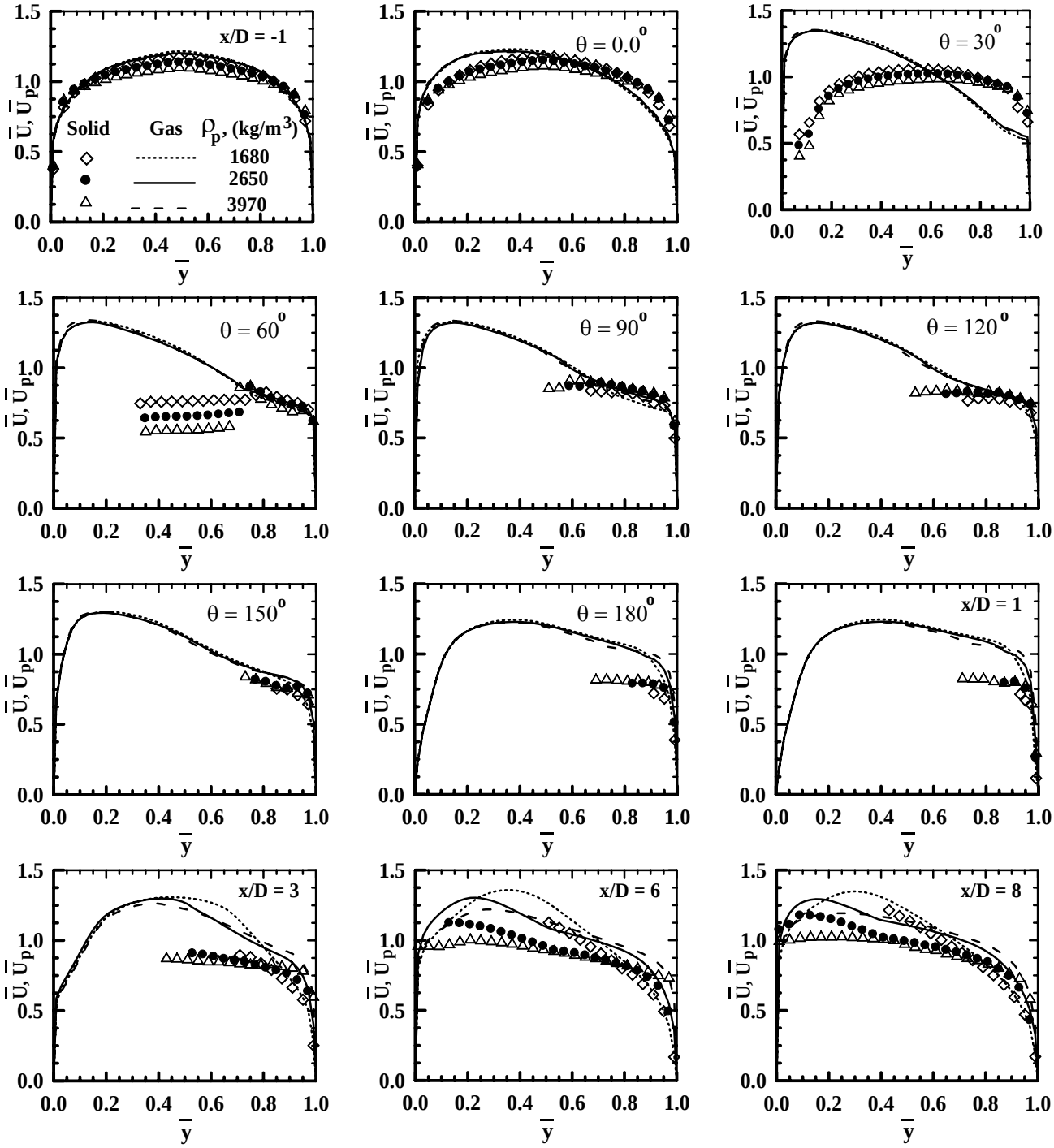

Fig. 9 Effect of particle density, ρ_p on the normalized axial velocity profiles for both phases.

Copyright © 2007 by ASME